

Role of trajectory symmetry in solid high-order harmonic generation

Shuang Wang(王爽), Yu Zhao(赵宇), Hui-Rong Wang(王慧荣), Yun-He Xing(邢云鹤), Xiao-Xin Huo(霍晓鑫), and Jun Zhang(张军)

Citation: Chin. Phys. B, 2026, 35 (**4**): 044204. DOI: 10.1088/1674-1056/ae04da
http://cpb.iphy.ac.cn; http://iopscience.iop.org/cpb

What follows is a list of articles you may be interested in

Optical temporal interference model for investigation and manipulation of non-integer high-order harmonic generation

Zhao-Yue Meng(孟昭越), Yun Pan(潘云), Jun-Ping Wang(王军平), and Xi Zhao(赵曦)
Chin. Phys. B, 2026, 35 (**2**): 024208. DOI: 10.1088/1674-1056/adfdc5

3D-GTDSE: A GPU-based code for solving 3D-TDSE in Cartesian coordinates

Ke Peng(彭科), Aihua Liu(刘爱华), Jun Wang(王俊), and Xi Zhao(赵曦)
Chin. Phys. B, 2025, 34 (**9**): 094203. DOI: 10.1088/1674-1056/adee00

Elliptically polarized high-order harmonic generation of Ar atom in an intense laser field

Jie Hu(胡杰), Yi-Chen Wang(王一琛), Qiu-Shuang Jing(景秋霜), Wei Jiang(姜威), Ge-Wen Wang(王革文), Yi-Wen Zhao(赵逸文), Bo Xiao(肖礴), Hong-Jing Liang(梁红静), and Ri Ma(马日)
Chin. Phys. B, 2024, 33 (**5**): 054208. DOI: 10.1088/1674-1056/ad2604

Tunable spectral continuous shift of high-order harmonic generation in atoms by a plasmon-assisted shaping pulse

Yuan Wang(王源), Yulong Li(李玉龙), Yue Qiao(乔月), Na Gao(高娜),Fu-Ming Guo(郭福明), Zhou Chen(陈洲), Lan-Hai He(赫兰海),Yu-Jun Yang(杨玉军), Xi Zhao(赵曦), and Jun Wang(王俊)
Chin. Phys. B, 2024, 33 (**3**): 034212. DOI: 10.1088/1674-1056/ad10fb

Spectral shift of solid high-order harmonics from different channels in a combined laser field

Dong-Dong Cao(曹冬冬), Xue-Fei Pan(潘雪飞), Jun Zhang(张军), and Xue-Shen Liu(刘学深)
Chin. Phys. B, 2023, 32 (**3**): 034204. DOI: 10.1088/1674-1056/aca4bf

---

Role of trajectory symmetry in solid high-order harmonic generation

Shuang Wang(王爽)[1], Yu Zhao(赵宇)[1], Hui-Rong Wang(王慧荣)[1], Yun-He Xing(邢云鹤)[1], Xiao-Xin Huo(霍晓鑫)[2], and Jun Zhang(张军)[1,†]

[1] *Institute of Atomic and Molecular Physics, Jilin University, Changchun* 130012, *China*
[2] *School of Science, Shenyang Ligong University, Shenyang* 110159, *China*

(Received 30 August 2025; revised manuscript received 30 August 2025; accepted manuscript online 9 September 2025)

High-order harmonic generation (HHG) from a ZnO crystal has been investigated theoretically using a two-band model driven by a few-cycle laser pulse. We observe that harmonics in the cut-off region exhibit periodic frequency shifts with changes in the carrier envelope phase (CEP) of the laser field. When the CEP of the laser pulse is an integer multiple of π, the cut-off region is dominated by even-order harmonics rather than odd-order harmonics. To illustrate the physical mechanism behind the even-order harmonics, we track the trajectories of electrons and holes between two successive half-cycles by performing time-frequency analysis and applying the recollision model. The results show that the maximum electron displacement is symmetric between successive half-cycles for odd-order harmonics. In contrast, the half-cycle symmetry of the maximum displacement is broken in the case of even-order harmonics.

Keywords: high-order harmonic generation, recollision model, trajectory analyses

PACS: 42.65.Ky, 32.80.Rm, 42.65.Re

DOI: 10.1088/1674-1056/ae04da **CSTR:** 32038.14.CPB.ae04da

1. Introduction

High-order harmonic generation (HHG) is a highly nonlinear phenomenon arising from the interaction between intense laser fields and matter. HHG from gases is one of the main sources for generating soft x-ray attosecond pulses and can be applied to probe ultrafast electron dynamics with attosecond time resolution.[1–3] However, the low electron density in gases results in weak harmonic conversion efficiency, which limits their practical applications. Recently, HHG from solids has attracted considerable attention due to its higher conversion efficiency and the possibility of reconstructing the band structure of semiconductors all-optically.[4–9] HHG from solids exhibits a range of novel phenomena, including the field dependence of maximum photon energy,[4,10] multiple plateaus in the harmonic spectrum,[11,12] and complex ellipticity dependence.[13,14] Furthermore, various crystals have been used as target materials to generate high-order harmonics,[15–17] making HHG in solids a hot research topic in recent years.

The mechanism of HHG in solids can be interpreted in terms of intraband currents and interband polarization.[5] The intraband current arises from the motion of electrons or holes within a single energy band, whereas the interband polarization is similar to atomic HHG and can be described using a recollision model.[5,18,19] In this model, HHG from solids involves three steps: (1) an electron is excited vertically from the top of the valence band (VB) to the conduction band (CB), creating an electron–hole pair; (2) the electron and hole are accelerated within their respective bands by the electric field; (3) the electron recollides with the hole, emitting a harmonic photon with energy determined by the band gap. Based on this model, a linear relationship between the cut-off energy of the harmonics and the electric field intensity can be theoretically established.[20]

Due to the inversion symmetry of the medium and the time-translation symmetry of the laser pulse, the harmonic spectrum of a solid typically contains only odd-order harmonics.[19–22] In particular, even-order harmonics cannot be directly generated in ZnO using only a two-band model.[23–26] Nevertheless, both odd- and even-order harmonics have been observed experimentally under certain conditions.[27–29] For example, Liu *et al.*[27] detected even-order harmonics from monolayer MoS_2, showing that the anomalous intraband current originating from the Berry curvature is responsible for their generation. Vampa *et al.*[28] observed even-order harmonics in ZnO driven by a combined linearly polarized laser field. The addition of a second harmonic breaks the symmetry of electron trajectories between successive half-cycles, leading to even-order harmonic generation. Many theoretical studies have also explored the underlying physics of even-order harmonics.[26,30–32] Jia *et al.*[26] used a multiple-band model to illustrate that even-order harmonics originate from electrons being excited to higher conduction bands in a stepwise process. Jiang *et al.*[30,31] highlighted the role of the transition dipole phase (TDP) and symmetry breaking, showing that nonzero TDP in a symmetry-broken solid leads to even harmonics. Across these investigations, odd-

†Corresponding author. E-mail: junzhang@jlu.edu.cn

© 2026 Chinese Physical Society and IOP Publishing Ltd. All rights, including for text and data mining, AI training, and similar technologies, are reserved.

and even-order harmonics typically appear alternately across the harmonic spectrum.[4,26,28–32]

In this work, we investigate HHG from ZnO along the Γ–M direction driven by a few-cycle laser pulse. We find that both odd- and even-order harmonics appear when the carrier envelope phase (CEP) of the laser field is an integer multiple of π, with even-order harmonics dominating the cut-off region. By analyzing electron trajectories in real space, we reveal that the asymmetry of electron maximum displacement between successive half-cycles is responsible for the generation of even-order harmonics. The paper is organized as follows: Section 2 describes the theoretical approach, Section 3 presents the simulation results and discussion, and Section 4 concludes the work.

2. Method

Since the time-dependent Schrödinger equation (TDSE) is primarily applied to model solids,[11,33] it cannot fully describe real solid materials. At present, simulations of laser interaction with real solids are mainly performed by solving the semiconductor Bloch equations (SBEs)[19,20,28,34] or using time-dependent density functional theory (TDDFT).[35,36] Approaches such as TDSE and TDDFT, however, do not account for dephasing effects. Therefore, in this work, we employ SBEs within a two-band model to describe the interaction between laser pulses and ZnO crystal. Unless stated otherwise, atomic units are used throughout. The SBEs are given by

$$\dot{n}_m = \mathrm{i}\sum_{m'\neq m}\Omega_{mm'}\pi_{mm'}\mathrm{e}^{\mathrm{i}S_{mm'}} + \mathrm{c.c.}, \tag{1}$$

$$\begin{aligned}\dot{\pi}_{mm'} = &-\frac{\pi_{mm'}}{T_2} + \mathrm{i}\Omega^*_{mm'}(n_m - n_{m'})\mathrm{e}^{-\mathrm{i}S_{mm'}} \\ &+\mathrm{i}\sum_{m''\notin\{m,m'\}}\Big(\Omega_{m'm''}\pi_{mm''}\mathrm{e}^{\mathrm{i}S_{m'm''}} \\ &-\Omega^*_{mm''}\pi^*_{m'm''}\mathrm{e}^{-\mathrm{i}S_{mm''}}\Big),\end{aligned} \tag{2}$$

where $n_m(\boldsymbol{K},t)$ is the population of band m (c for conduction band, v for valence band), with all electrons initially in the valence band. $\Omega_{mm'}(\boldsymbol{K},t) = \boldsymbol{E}(t)\cdot\boldsymbol{d}_{mm'}[\boldsymbol{K}+\boldsymbol{A}(t)]$ is the polarization strength, where $\boldsymbol{d}_{mm'}$ is the transition dipole moment.[20] The crystal momentum $\boldsymbol{k}$ is transformed to a moving frame via $\boldsymbol{K} = \boldsymbol{k} - \boldsymbol{A}(t)$,[37] shifting the first Brillouin zone (BZ) to $\overline{\mathrm{BZ}} = \mathrm{BZ} - \boldsymbol{A}(t)$, with the BZ defined as $[-\pi/a, \pi/a]$ and lattice constant $a = 5.32$ a.u. The classical action is $S_{mm'}(\boldsymbol{K},t) = \int_{-\infty}^{t}\varepsilon_{mm'}[\boldsymbol{K}+\boldsymbol{A}(t')]\mathrm{d}t'$, where $\varepsilon_{mm'} = E_m - E_{m'}$ is the band energy difference. Following experimental comparison, the dephasing time is set as $T_2 = 1.375$ fs to effectively remove anharmonic contributions in the high-order harmonics.[5,23,25] Different from Ref. [38], the system is not allowed to exchange energy with phonons of lattice defects in this work. Thus, $T_2 = 1.375$ fs is adopted to depict the intrinsic dephasing time of the ZnO crystal.

The intraband and interband harmonic spectra are obtained by Fourier transform of the corresponding currents

$$S_{\mathrm{intra}}(\omega) = \omega^2\left|\int \boldsymbol{j}_{\mathrm{intra}}(t)\mathrm{e}^{-\mathrm{i}\omega t}\mathrm{d}t\right|^2, \tag{3}$$

$$S_{\mathrm{inter}}(\omega) = \omega^2\left|\int \boldsymbol{j}_{\mathrm{inter}}(t)\mathrm{e}^{-\mathrm{i}\omega t}\mathrm{d}t\right|^2. \tag{4}$$

The ZnO band structure is taken from Refs. [5,20], obtained via *ab initio* calculations under the local density approximation, with a bandgap $E_{\mathrm{g}} = 0.1213$ a.u. (3.3 eV) at the Γ point. The laser field is linearly polarized along the Γ–M direction

$$E(t) = E_0 f(t)\cos(\omega_0 t + \varphi), \quad f(t) = \cos^2\left(\frac{\pi t}{\tau}\right), \tag{5}$$

where τ is the pulse duration (5 optical cycles), $E_0 = 0.00342$ a.u. (4.1×10^{11} W/cm^2), $\omega_0 = 0.014$ a.u. (3253 nm), and φ is the CEP. The peak field is below the Bloch field $E_{\mathrm{b}} = \pi\omega_0/a \approx 0.008$ a.u., so excitation to higher conduction bands is neglected.[33]

3. Results and discussion

Figure 1 shows the intraband and interband harmonic spectra for a laser pulse with $\varphi = 0$. Odd-order harmonics dominate below the 24th harmonic due to inversion symmetry along the Γ–M direction,[19,20,22] while even-order harmonics (e.g., 24th and 26th) appear near the cut-off region. Solid HHG originates from intraband and interband currents. Intraband harmonics arise from Bloch oscillations and a recollision-like contribution associated with electron–hole polarization. Since intraband harmonics are weaker than interband ones by about four orders of magnitude near the cut-off, we focus primarily on interband harmonics. Unlike previous works where odd- and even-order harmonics appear alternately across the entire spectrum,[26–28] in our case, even-order harmonics appear only near the cut-off. Because the system retains inversion symmetry, the phase of $\boldsymbol{d}_{mm'}$ is set to zero,[21,39] differing from scenarios with nonzero transition dipole phase that generate even-order harmonics.[30,31] The physical mechanism for this observation warrants further investigation.

The Bloch oscillation of electrons depends on the vector potential of the driving pulse, i.e., $\boldsymbol{K} = \boldsymbol{k} - \boldsymbol{A}(t)$. Changing the CEP of the laser field alters the waveform of the vector potential, thereby controlling the motion of Bloch electrons and directly modifying their acquired kinetic energy ε ($\varepsilon \propto [A_{\mathrm{b}}(t) - A_{\mathrm{r}}(t)]^2$, where t_{b} and t_{r} denote the birth and recollision times).[40–43] We further investigate the influence of CEP on HHG in both the plateau and cut-off regions. Figure 2(a) shows the CEP dependence of the harmonics in the plateau region (9th–15th harmonics), where the harmonics exhibit negligible dependence on CEP. In contrast, in the cut-

off region, the harmonics continuously shift with CEP variation, as presented in Fig. 2(b), indicating that the generation of even-order harmonics is highly sensitive to CEP. Such a distinction between plateau and cut-off regions has also been observed in topological insulators,[41] where it is attributed to the ballistic acceleration of Dirac currents in the topological surface state. As seen in Fig. 2(b), when CEP is a half-integer multiple of π, odd-order harmonics dominate the cut-off region. Conversely, even-order harmonics are generated when CEP is an integer multiple of π. To elucidate the mechanism of even-order harmonic emission, we focus on trajectory analysis for the specific case of $\varphi = 0$, which exhibits clear even-order harmonics.

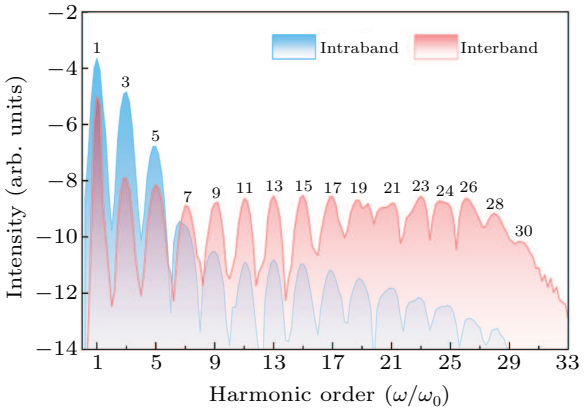


Fig. 1. Intra- and interband harmonic spectra driven by a few-cycle laser pulse. The laser field has an amplitude of 0.00342 a.u., a frequency of 0.014 a.u., and a duration of 5 optical cycles (o.c.).

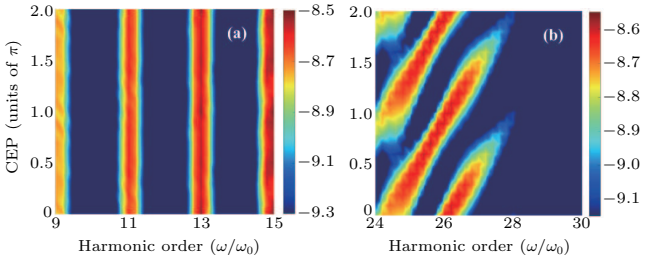


Fig. 2. CEP dependence of high-order harmonics from ZnO: (a) 9th–15th order harmonics and (b) 24th–30th order harmonics. The other laser parameters are the same as those in Fig. 1.

To gain a deeper physical insight into the even-order harmonics, we present the time-frequency (TF) distribution of HHG through the Morlet wavelet transformation[44] in Fig. 3(a). It can be seen that the generation of harmonics occurs mainly at the center of the laser pulse, with two primary peaks contributing to harmonic generation, marked as P_1 and P_2, respectively. For harmonics below the 25th order, the short trajectories from P_1 and P_2 contribute together. However, for harmonics above the 26th order, the emission mainly originates from a single short trajectory of P_1. Moreover, Fig. 3(a) shows that the temporal separation between these two bursts increases with harmonic order, resulting in a time delay between successive subcycles during harmonic emission. In the harmonic spectra, this gives rise to peaks separated by slightly less than twice the laser frequency.[40]

In Ref. [40], the instantaneous energy difference was calculated to understand harmonic emission dynamics. The results indicate that harmonic orders deviate from odd multiples when the vector potential peaks at the envelope maximum. Comparing with Fig. 3(a) in Ref. [40], the instantaneous energy difference agrees with the TF distribution. Furthermore, the energy difference approximately traces the magnitude of the vector potential $|A(t)|$.[45]

Figure 3(a) also illustrates the magnitude of the vector potential $|A(t)|$ (magenta dashed lines), used to trace the instantaneous energy difference. A time delay is observed between each emission path and the vector potential, which arises because only the Γ point ($\boldsymbol{k} = 0$) is considered in TDSE calculations of Ref. [40]. In this work, we investigate HHG in ZnO crystal by solving the SBEs, considering a fully occupied valence band (all crystal momenta within the first BZ). Thus, the mechanism of even-order harmonic generation may differ from that in Ref. [40]. TF analysis of the Γ channel (not shown here) also follows the vector field magnitude, consistent with Ref. [40].

Figure 3(b) depicts the harmonic orders as a function of birth time and recollision time calculated by the recollision model derived from a fully occupied VB, consistent with Refs. [18–20]. Two main peaks, P_1 and P_2, contribute to HHG, in agreement with TF analysis from SBEs shown in Fig. 3(a). Peak P_2 does not contribute to harmonics above the 25th order, whereas harmonics below the 25th arise from both P_1 and P_2. The red dotted line in Fig. 3(b) shows the transient CB population. The CB population rapidly increases from $t = -0.75$ o.c. to $t = -0.25$ o.c., corresponding to the birth time of P_1', and recombines at $t = -0.25$ o.c. to $t = 0.25$ o.c. Similarly, from $t = -0.25$ o.c. to $t = 0.15$ o.c., the CB population rises again, corresponding to the birth of P_2', with recombination from 0.25 o.c. to 0.65 o.c.

To further understand even-order harmonic generation, we analyze electron trajectories between two successive half-cycles using the recollision model.[18,19,46] For all harmonic orders, we set the initial condition at the Γ point ($\boldsymbol{k} = 0$). Figures 4(a1) and 4(a2) show trajectories of the electron and its associated hole for the 13th harmonic at different birth times t_b. In Fig. 4(a1), the electron–hole pair is created at $t_b = -0.35$ o.c. (peak P_1' from Fig. 3(b)), with the electron and hole moving along positive- and negative-X directions, respectively. At $t_r = -0.05$ o.c., the electron recollides with the hole, emitting a harmonic photon. The maximum displacement of the electron is around $X = 0.85$ a.u. In Fig. 4(a2), the pair is created at $t_b = 0.15$ o.c., recolliding at $t_r = 0.45$ o.c., with maximum displacement $X = -0.85$ a.u. The electron thus moves

symmetrically in positive- and negative-X directions over successive half-cycles. As proposed by Vampa *et al.*,[47] HHG can be viewed as an array of interferometers, with each arm corresponding to electron–hole trajectories generated in subsequent half-cycles. Equal electron propagation distances lead to constructive interference only for odd-order harmonics, here generating the 13th harmonic.

Figures 4(b1) and 4(b2) show electron trajectories for the 15th harmonic. The maximum displacements are $X = 1.23$ a.u. and $X = -1.23$ a.u., symmetric over successive half-cycles. Compared with the 13th harmonic, the electron gains more energy due to the longer displacement, and the symmetry ensures the generation of the 15th harmonic.

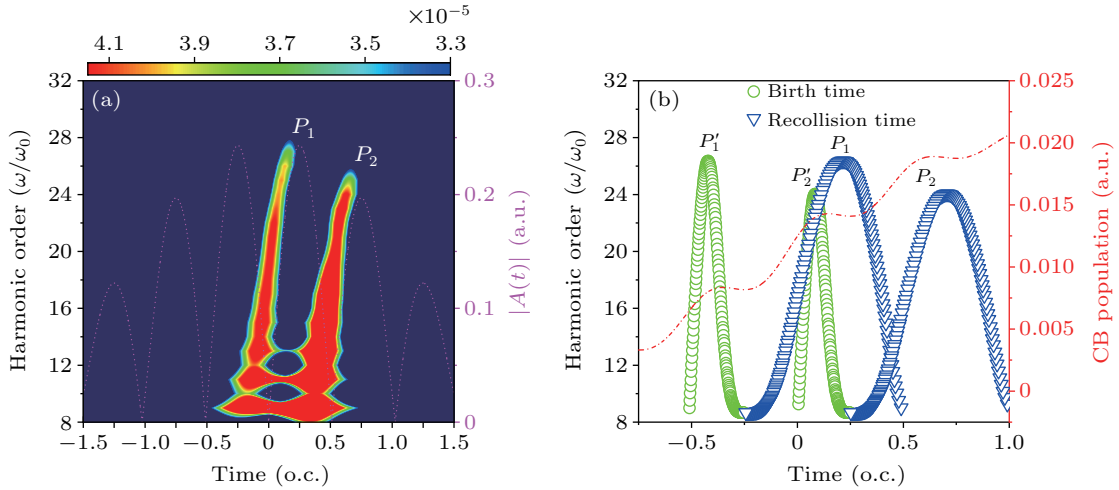


Fig. 3. (a) Time-frequency distribution of the interband HHG spectrum with a logarithmic color scale. The magenta dashed lines represent the magnitude of the vector potential $|A(t)|$. (b) Harmonic orders as a function of birth time (green circles) and recollision time (blue triangles) calculated by the recollision model. The red dotted line shows the time-dependent conduction band (CB) population.

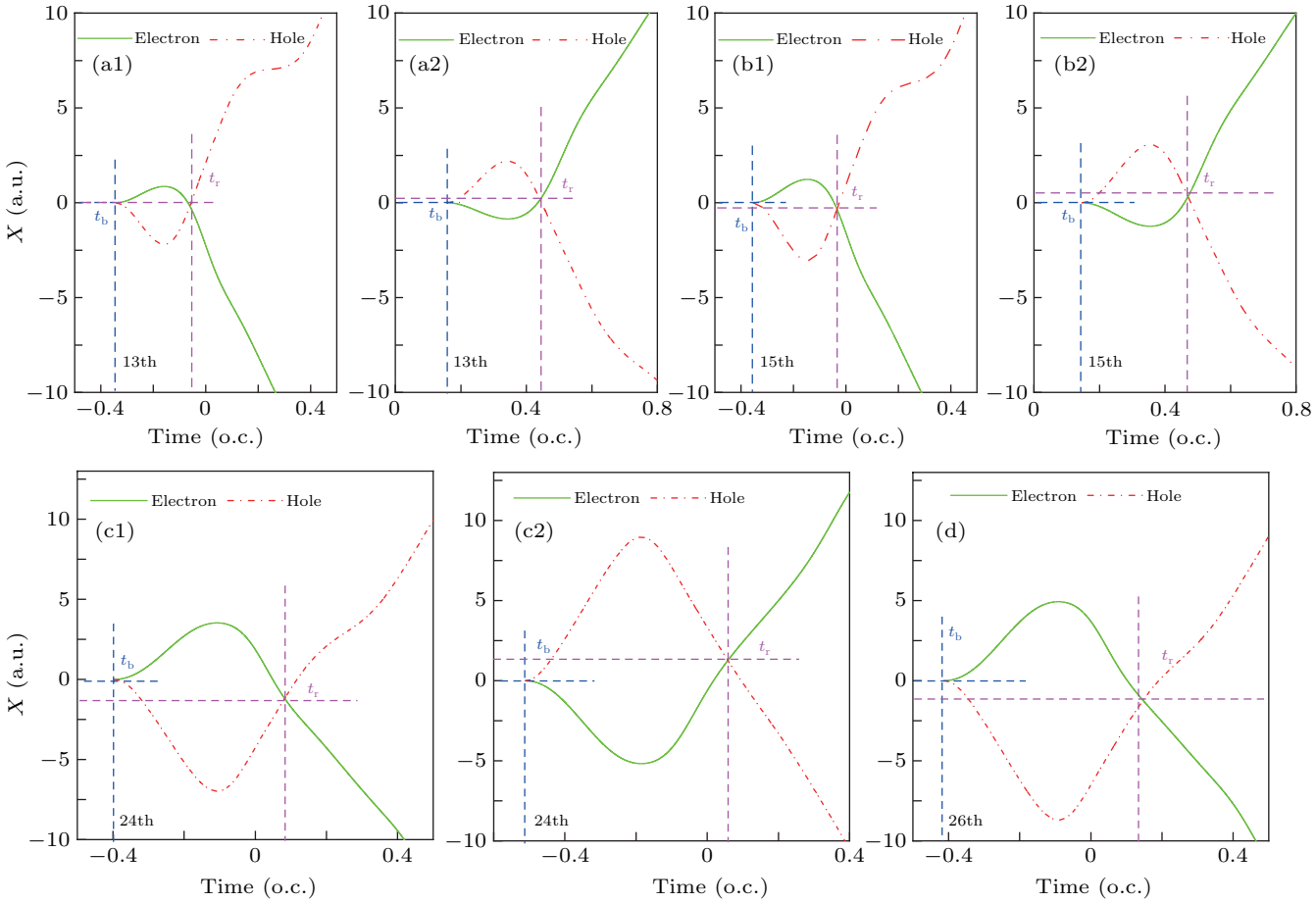


Fig. 4. (a1) and (a2) Trajectories of the electron (green solid line) and hole (red dotted-dashed line) born at different times for the 13th harmonic in real space. (b1) and (b2) Same as (a1) and (a2) but for the 15th harmonic. (c1) and (c2) Same as (a1) and (a2) but for the 24th harmonic. (d) Trajectories of the electron (green solid line) and hole (red dotted-dashed line) for the 26th harmonic in real space.

Figures 4(c1) and 4(c2) illustrate the trajectories of the electron and associated hole for the 24th harmonic between two successive half-cycles. From Fig. 4(c1), the electron–hole pair is created at $t_b = -0.40$ o.c. (peak P_1' in Fig. 3(b)). The electron recollides with its associated hole at $t_r = 0.08$ o.c., with a maximum displacement of $X = 3.52$ a.u. From Fig. 4(c2), the electron–hole pair is created at $t_b = 0.09$ o.c. (peak P_2' in Fig. 3(b)) and recollides at $t_r = 0.66$ o.c., with a maximum displacement $X = -5.17$ a.u. in the negative-X direction. The asymmetry of maximum displacement between two successive half-cycles leads to constructive interference for even-order harmonics, e.g., the 24th harmonic, following Eq. (33) in Ref. [47]. Figure 4(d) shows the trajectory of the 26th harmonic, where the electron moves only in the positive-X direction with a maximum displacement of $X = 4.93$ a.u., confirming that even-order harmonics originate from asymmetric electron trajectories.

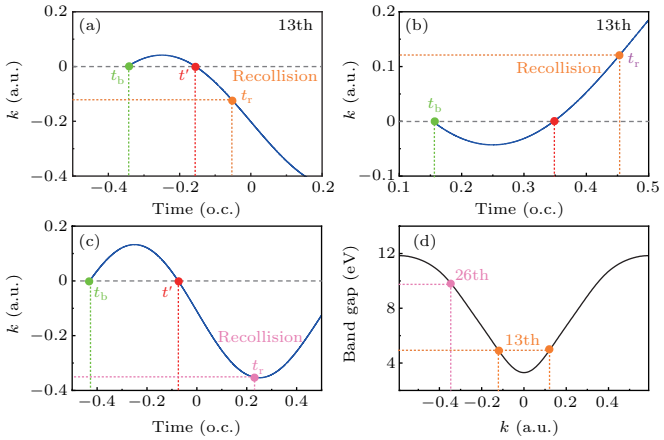


Fig. 5. (a) and (b) Trajectories of electrons for the 13th harmonic in $\boldsymbol{k}$-space. The birth times correspond to those in Figs. 4(a1) and 4(a2), respectively. (c) Trajectories in $\boldsymbol{k}$-space for the 26th harmonic; the birth time corresponds to Fig. 4(d). (d) Band gap between the VB and CB in $\boldsymbol{k}$-space, with markers indicating the recollision points for the 13th (orange) and 26th (pink) harmonics.

To further elucidate the HHG dynamics, we analyze electron and hole trajectories in $\boldsymbol{k}$-space using the recollision model.[18] Figures 5(a) and 5(b) depict the $\boldsymbol{k}$-space trajectories for the 13th harmonic, corresponding to birth times in Figs. 4(a1) and 4(a2). In Fig. 5(a), the electron–hole pair is created at $\boldsymbol{k} = 0$ (green point), then undergoes Bloch oscillation driven by the laser pulse. At $t = t'$, the electron and hole pass through $\boldsymbol{k} = 0$ (red point) and finally recollide at $\boldsymbol{k} = -0.12$ a.u. (orange point). In Fig. 5(b), the electron recollides at $\boldsymbol{k} = 0.12$ a.u. (orange point). For odd-order harmonics, the crystal momentum of recollision is symmetric about the Γ point.

Figure 5(c) shows the $\boldsymbol{k}$-space trajectory for the 26th harmonic (birth times in Fig. 4(d)). Only a single trajectory contributes, with recollision at $\boldsymbol{k} = -0.35$ a.u. (pink point), resulting in loss of half-cycle symmetry for even-order harmonics. Figure 5(d) presents the band gap between CB and VB in $\boldsymbol{k}$-space. The two orange points correspond to the band gap at $\boldsymbol{k} = -0.12$ a.u. and $\boldsymbol{k} = 0.12$ a.u. (energy ~ 4.35 eV, 13th harmonic), while the pink point represents the band gap at $\boldsymbol{k} = -0.35$ a.u. (energy ~ 9.91 eV, 26th harmonic).

4. Conclusion

In summary, we investigated the HHG from ZnO crystal within the framework of a two-band model. By tuning the CEP of the incident pulse, we observed even-order harmonics in the cut-off region when the CEP is integer multiples of π. To investigate the electron dynamics of harmonic generation, we analyzed the electron trajectories in real space using the recollision model. It is demonstrated that the even-order harmonic generation is a consequence of the asymmetry of the maximum displacement of the electron between two successive half-cycles. We also analyzed the recollision dynamics of the electron–hole pair in the $\boldsymbol{k}$-space. The results show that the crystal momentum when the electron recollides with its associated hole is symmetric about the Γ point for odd-order harmonics, while it is asymmetric for even-order harmonics. We expect that our results will contribute to further exploration and understanding of the physical mechanisms of solid HHG.

Acknowledgments

This work was supported by the Natural Science Foundation of Jilin Province of China (Grant No. 20230101014JC) and the National Natural Science Foundation of China (Grant No. 12374265).

References

[1] L'Huillier A and Balcou P 1993 *Phys. Rev. Lett.* **70** 774
[2] Corkum P B 1994 *Phys. Rev. Lett.* **71** 1993
[3] Zhang J, Ge X L, Wang T, Xu T T, Guo J and Liu X S 2015 *Phys. Rev. A* **92** 013418
[4] Ghimire S, DiChiara A D, Sistrunk E, Agostini P, DiMauro L F and Reis D A 2011 *Nat. Phys.* **7** 138
[5] Vampa G, McDonald C R, Orlando G, Klug D D, Corkum P B and Brabec T 2014 *Phys. Rev. Lett.* **113** 073901
[6] Qiao Y, Chen J Q, Zhou S S, Chen J G, Jiang S C and Yang Y J 2024 *Chin. Phys. Lett.* **41** 014205
[7] Luu T T, Garg M, Kruchinin S Yu, Moulet A, Hassan M Th and Goulielmakis E 2015 *Nature* **521** 498
[8] Garg M, Kim H Y and Goulielmakis E 2018 *Nat. Photonics* **12** 291
[9] Vampa G, Hammond T J, Thiré N, Schmidt B E, Légaré F, McDonald C R, Brabec T, Klug D D and Corkum P B 2015 *Phys. Rev. Lett.* **115** 193603
[10] Ikemachi T, Shinohara Y, Sato T, Yumoto J, Kuwata-Gonokami M and Ishikawa K L 2017 *Phys. Rev. A* **95** 043416 2020 *Chin. Phys. B* **29** 104206
[11] Wu M X, Ghimire S, Reis D A, Schafer K J and Gaarde M B 2015 *Phys. Rev. A* **91** 043839
[12] Yu C, Iravani H and Madesen L B 2020 *Phys. Rev. A* **102** 033105
[13] Tancogne-Dejean N, Müecke O D, Kärtner F X and Rubio A 2017 *Nat. Phys.* **8** 745
[14] You Y S, Reis D A and Ghimire S 2017 *Nat. Commun.* **13** 345
[15] Klemke N, Mücke O D, Rubio A, Kärtner F X and Tancigne-Dejean N 2020 *Phys. Rev. B* **102** 104308
[16] Li J, Lu J, Chew A, Han S. Li J, Wu Y, Wang H, Ghimire S and Chang Z 2020 *Nat. Commun.* **11** 2748

[17] Hohenleutner M, Langer F, Schubert O, Knorr M, Huttner U, Koch S W, Kira M and Huber R 2015 *Nature* **523** 572
[18] Fu S, Feng Y, Li J, Yue S, Zhang X, Hu B and Du H 2020 *Phys. Rev. A* **101** 023402
[19] He Y L, Guo J, Gao F Y, Yang Z J, Zhang S Q and Liu X S 2021 *Phys. Rev. A* **104** 013104
[20] Vampa G, McDonald C R, Orlando G, Corkum P B and Brabec T 2015 *Phys. Rev. B* **91** 064302
[21] Wang S, Liu S T, Huo X X, Xing Y H and Zhang J 2023 *Phys. Rev. A* **108** 063106
[22] Neufeld O, Podlsky D and Cohen O 2019 *Nat. Commun.* **10** 405
[23] Luu T T and Wörner H J 2016 *Phys. Rev. B* **94** 115164
[24] Yu C, Jiang S and Lu R 2019 *Adv Phys: X* **4** 1562982
[25] Wu T, Qian C, Wang Z, Zhang X, Yu C and Lu R 2022 *Acta Photonica Sinica* **51** 0851515
[26] Jia G R, Huang X H and Bian X B 2017 *Opt. Express* **25** 23654
[27] Liu H, Li Y, You Y S, Ghimire S, Heinz T F and Reis D A 2017 *Nat. Phys.* **13** 262
[28] Vampa G, Hammond T J, Thiré N, Schmidt B E, Légaré F, McDonald C R, Brabec T and Corkum P B 2015 *Nature* **522** 4622
[29] Schubert O, Hohenleutner M, Langer F, Urbanek B, Lange C, Huttner U, Golde D, Meier T, Kira M, Koch S W and Huber R 2014 *Nat. Photonics* **8** 119
[30] Jiang S, Chen J, Wei H, Yu C, Lu R and Lin C D 2018 *Phys. Rev. Lett.* **120** 253201
[31] Jiang S, Wei H, Chen J, Yu C, Lu R and Lin C D 2017 *Phys. Rev. A* **96** 053850
[32] Jiang S, Gholam-Mirzaei S, Crites E, Beetar J E, Singh M, Lu R, Chini M and Lin C D 2019 *J. Phys. B: At. Mol. Opt. Phys.* **52** 225601
[33] Wang X Q, Xu Y, Huang X H and Bian X B 2018 *Phys. Rev. A* **98** 023427
[34] McDonald C R, Vampa G, Corkum P B and Brabec T 2015 *Phys. Rev. A* **92** 033845
[35] Yabana K, Sugiyama T, Shinohara Y, Otobe T and Bertsch G F 2012 *Phys. Rev. B* **85** 045134
[36] Floss I, Lemell C, Wachter G, Smejkal V, Sato A S, Tong X M, Yabana K and Burgdörfer J 2018 *Phys. Rev. A* **97** 011401
[37] Bloch F 1929 **52** 555 1929 *Z. Phys.* **52** 555
[38] Floss I, Lemell C, Yabana K and Burgdörfer 2019 *Phys. Rev. B* **99** 224301
[39] Li J, Zhang X, Fu S, Feng Y, Hu B and Du H 2019 *Phys. Rev. A* **100** 043404
[40] You S Y, Wu M X, Yin Y, Chew A, Ren X, Gholam-Miezaei S, Browne D A, Chini M, Chang Z, Schafer K J, Gaared M B and Ghimire S 2017 *Opt. Lett.* **42** 1816
[41] Schmid C P, Weigl L, Grössing P, Junk V, Gorini C, Schlauderer S, Ito S, Meierhofer M, Hofmann N, Afanasiev D, Crewse J, Kokh K A, Tereshchrnko O E, Güdde J, Evers F, Wilhelm J, Richter K, Höfer U and Huber R 2021 *Nature* **593** 385
[42] Shirai H, Kumaki F, Nomura Y and Fuji T 2018 *Opt. Lett.* **43** 2094
[43] Graml M, Nitsch M, Seith A, Evers F and Wilhelm J 2023 *Phys. Rev. B* **107** 054305
[44] Ashmead J 2012 *Quanta* **1** 58
[45] Wu M X, Browne D A, Schafer K J and Gaarde M B 2016 *Phys. Rev. A* **94** 063403
[46] Zhang X, Li J, Zhou Z, Yue S, Du H, Fu L and Luo H G 2019 *Phys. Rev. B* **99** 014304
[47] Vampa G and Brabec T 2017 *J. Phys. B: At. Mol. Opt. Phys.* **50** 083001